

Complementary Model Update: A Method for Simultaneous Registration and Stiffness Mapping in Flexible Environments

Rangaprasad Arun Srivatsan¹, Elif Ayvali¹, Long Wang², Rajarshi Roy², Nabil Simaan² and Howie Choset¹

Abstract— Registering a surgical tool to an *a priori* model of the environment is an important first step in computer-aided surgery. In this paper we present an approach for simultaneous registration and stiffness mapping using blind exploration of flexible environments. During contact-based exploration of flexible environments, the physical interaction with the environment can induce local deformation, leading to erroneous registration if not accounted for. To overcome this issue, a new registration method called complementary model update (CMU), is introduced. By incorporating measurements of the contact force, and contact location, we minimize a unique objective function to cancel out the effect of local deformation. We are thus able to acquire the necessary registration parameters using both geometry and stiffness information. The proposed CMU method is evaluated in simulation and using experimental data obtained by probing silicone models and an *ex vivo* organ.

I. INTRODUCTION

Minimally invasive surgery (MIS) has the potential to reduce patient trauma, post-operative complications, recovery time and cost. Unfortunately, surgical navigation remains a challenging task in MIS, and hence computer aided surgery (CAS) was developed to assist surgeons in overcoming this challenge. A prerequisite for successful CAS is an accurate registration of pre-operative images to intra-operative anatomy. Typically, prior work relied on image guided techniques [1] while others used structured light [2] and force-based exploration [3], [4]. In this paper, we pursue the concept of sensory-guided surgery based on force/contact exploration in flexible environments.

In our prior work [5], we address simultaneous compliance and registration estimation (SCAR) using a filtering approach. However, the filtering implementation for SCAR is not robust to initialization error, and therefore we have developed a new update model, termed complementary model update (CMU) that can be used to accurately estimate the registration, in a filtering approach as well as using a generic non-linear optimizer. This update model encodes both contact force and contact location information.

The use of contact/force data comes with the advantage of providing stiffness information, which can enhance the performance and robustness of registration. This advantage however comes at a cost of having to consider the induced

*This work was supported by NRI Large grants IIS-1426655 and IIS-1327566

¹R. A. Srivatsan, E. Ayvali, H. Choset are with the Robotics Institute at Carnegie Mellon University, Pittsburgh, PA 15213, USA (rarunsrivatsan@, eayvali@, choset@cs.) cmu.edu

²L. Wang, R. Roy and N. Simaan are with the Department of Mechanical Engineering, Vanderbilt University, Nashville, TN 37235, USA (long.wang, rajarshi.roy, nabil.simaan) @vanderbilt.edu

local surface deformation due to the physical interaction of the surgical tool with the organ. In this work, we simultaneously use multiple position-force measurements to estimate the local deformation, which is then used to estimate the local stiffness as well as registration parameters. While existing approaches in literature perform mechanical palpation to find tissue stiffness (e.g. [3], [4], [6]), we are interested in using the stiffness properties to improve the registration estimate.

The performance of the proposed formulation is evaluated for various geometries, stiffness distributions, subject to sensor noise levels and initial conditions. The new formulation is validated with simulated data and experimental data obtained by palpating a silicone phantom organ and an *ex vivo* organ. A simple experimental setup consisting of a surgical tool that can sense force and position at its tip is used to validate the core ideas for the use of contact/force based exploration data for registration. Ultimately, we show that the CMU approach overcomes the aforementioned issues associated with local deformations due to contact exploration and offers improved performance compared to other known methods. We believe this approach can be used in MIS for resection or ablation of tumors in organs such as liver, bladder and kidneys [7].

II. RELATED WORK

When the anatomy is rigid, registration yields the homogeneous transformation matrix that relates points in the anatomy's frame to the frame of its *a priori* model. One of the most popular techniques for rigid registration is the iterative closest point (ICP) [8]. Improvements over the original ICP have been developed which deal with outlier detection [9], fast computation [10] and handling noise in data [11] and overcoming local minima solutions [12].

When dealing with anatomy that is flexible, we observe discrepancy between the model of the source and the target due to the global deformation of the target caused by swelling or organ shift due to gravity and positioning of the patient. Non-rigid registration techniques, that are popularly referred to as “deformable registration” methods, have been developed to address this issue. Prior work such as [13], [14] and the references therein describe techniques to perform deformable registration. The majority of previous works relies on non-contact based methods to produce geometric data for registration. Techniques such as [15] use organ geometry and image processing to perform registration, but perform poorly when the visible organ is obfuscated with blood and also respond adversely to change in lighting.

Other imaging modalities such as intraoperative ultrasound (US) based registration for soft bodies [16], [17] deal with

registering the preoperative model to the US image, instead of the surgical tool. Methods such as [18] require a pre-registration step where either fiducial markers are used or an expert manually chooses points of interest from the US image to provide a good initial guess for the registration algorithm. Techniques such as [19] present a fiducial free way for registration using 3D ultrasound (3DUS). Such methods depend heavily on finding distinctive 3DUS features which may not be successful in every surgical scenario.

To the best of our knowledge, the only work that uses contact/force based blind exploration data to perform registration is our previous approach for SCAR [5]. An iterated extended Kalman filter (IEKF) was used to simultaneously estimate the registration parameters and generate a stiffness map of the environment. In Section IV we discuss some of the drawbacks of our previous implementation of SCAR and motivate the need for a more robust formulation.

III. PROBLEM STATEMENT AND ASSUMPTIONS

Given an *a priori* geometric model of an organ as well as the measurements of the tool tip positions and associated contact forces, (i) the surgical tool needs to be registered to the frame of the model, and (ii) the stiffness distribution over the organ's surface needs to be estimated. We make the following assumption in this work:

- i The true shape of the organ is not globally deformed but instead experiences local deformations only due to interaction with the tool.
- ii The tool-tip's position can be measured accurately.
- iii The tool has force sensing capability so that it can be servoed in a hybrid position-force control manner.
- iv The forces applied by the tool are within the admissible range (typically $\approx 1N$) in which the organ only undergoes a small deformation that allows it to realize its undeformed state when the force is removed.
- v The friction between the tool tip and the surface of the soft body is negligible.

IV. MODELING

Now, we describe the complementary model update (CMU) to simultaneously estimate the variation of stiffness over the surface as well as register a flexible environment to its *a priori* model. Our group had earlier developed a filtering approach for SCAR that was reported in [5]. For the rest of this paper, the old implementation of SCAR using IEKF will be referred to as SCAR-IEKF-old. SCAR-IEKF-old uses a geometric prior represented in the form of a triangular mesh and therefore each triangle was assigned its own stiffness values. The state vector \mathbf{x}_k consisted of six registration parameters and the stiffness values associated with each triangle of the triangular mesh. The update step involved using sensed position and force measurements to minimize the following objective function:

$$h_1(\mathbf{x}_k) = -(\mathbf{n}_j^C)^T (\mathbf{d}^C \mathbf{p}_j^C - \mathbf{u}^C \mathbf{p}_j^C) (c_i) \mathbf{x}_k + f_j, \quad (1)$$

$$\text{where } \mathbf{d}^C \mathbf{p}_j^C = \mathbf{T}_{\mathbf{x}_k} (\mathbf{d}^R \mathbf{p}_j^R). \quad (2)$$

TABLE I
NOTATIONS

Symbol	Description
$[.]^R$	Entities defined in robot's frame
$[.]^C$	Entity defined in model's frame
\mathbf{n}	Normal vector
$\mathbf{d}^C \mathbf{p}$	Coordinates of deformed point
$\mathbf{u}^C \mathbf{p}$	Coordinates of undeformed point
\mathbf{T}	Homogeneous transformation matrix
f	Force magnitude
c	Stiffness
d	Deformation depth
ϕ	CAD model

The position of the j^{th} deformed point is $\mathbf{d}^C \mathbf{p}_j^R$, measured in the robot frame ¹ and the corresponding sensed force is f_j . The corresponding closest point on the CAD model is $\mathbf{u}^C \mathbf{p}_j^C$ and the normal vector is \mathbf{n}_j^C . The objective function $h_1(\mathbf{x}_k)$ is the difference between the estimated force and the measured force. The objective function is minimized over \mathbf{x}_k and as mentioned above, \mathbf{T} , the homogeneous transformation matrix and c_i , the stiffness associated with triangle i (see notations in Table I) are obtained from \mathbf{x}_k and hence are updated simultaneously.

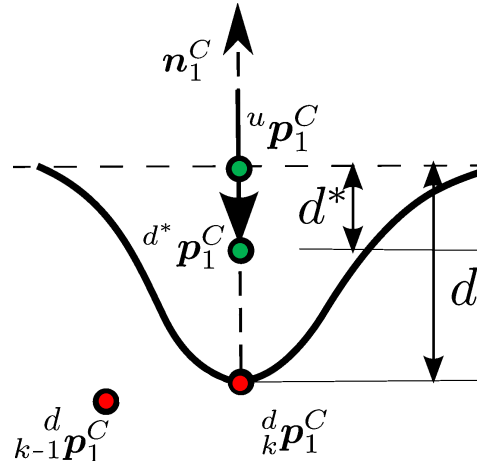


Fig. 1. Schematic shows ambiguity in single measurement based update

Fig. 1 shows the true location of the deformed point $d^* \mathbf{p}_1^C$ which is at a depth d^* along the normal \mathbf{n}_1^C . Let the location of the deformed point obtained from the registration estimate of previous iteration be $k-1 \mathbf{d}^C \mathbf{p}_1^C$ as shown in Fig. 1. The subscript $k-1$ indicates that the coordinates are transformed using the registration estimate from the previous iteration. After applying the state update using Eq. 1, the updated position of the deformed point is $k \mathbf{d}^C \mathbf{p}_1^C$, which is at a depth d along the normal (see Fig. 1). The filter estimates the stiffness value to be $c_i = \frac{f_j}{d} \neq \frac{f_j}{d^*} = c_i^*$. As can be observed from Eq. 1, substituting c_i and $k \mathbf{d}^C \mathbf{p}_1^C$ yields $h_1(\mathbf{x}_k) = 0$. Substituting c_i^* and $k \mathbf{d}^C \mathbf{p}_1^C$ in Eq. 1 also yields $h_1(\mathbf{x}_k) = 0$.

¹We assume that the tool is rigidly attached to the robot and hence transformation between the robot's frame and the tool's frame can be carried out trivially by a precomputed rigid transformation.

This results in an ambiguity in registration along the normal and an incorrect stiffness estimation.

We make an observation that when the registration is updated based on a pair of observations, the ambiguity in registration is resolved. Let us select two points, ${}^u\mathbf{p}_1^C$ and ${}^u\mathbf{p}_2^C$, on the undeformed surface of the organ that are spatially close to each other. Since the points are close to each other, we assume that the normals \mathbf{n}^C and the stiffness c at both locations are the same. Let us apply a force of magnitude f_1 and f_2 respectively at ${}^u\mathbf{p}_1^C$ and ${}^u\mathbf{p}_2^C$. Upon application of the force, the surface would deform by depths:

$$d_i = \frac{f_i}{c}, \quad i = 1, 2. \quad (3)$$

From Eq. 3, we have:

$$c = \frac{f_2 - f_1}{d_2 - d_1}, \quad \text{when } d_2 \neq d_1. \quad (4)$$

Let the coordinates of the deformed points be ${}^d\mathbf{p}_1^R$ and ${}^d\mathbf{p}_2^R$. From Eq. 4, stiffness $c = \frac{f_2 - f_1}{||{}^d\mathbf{p}_2^R - {}^d\mathbf{p}_1^R||}$. We can now relate the deformed and undeformed probed points from the linear stiffness model (see Fig. 1):

$$\begin{aligned} {}^u\mathbf{p}_1^C - \mathbf{n}^C d_1 &= {}^d\mathbf{p}_1^R \\ \Rightarrow {}^u\mathbf{p}_1^C - \mathbf{n}^C \frac{f_1}{c} &= \mathbf{T}({}^d\mathbf{p}_1^R), \end{aligned} \quad (5)$$

where $\mathbf{T}(\mathbf{p})$ transforms \mathbf{p} from tool-frame to CAD model-frame. The LHS of Eq. 5 is the estimated position of the deformed point in the CAD model frame based on the estimated stiffness c and the RHS is the coordinates of the sensed deformed points transformed to the CAD model frame.

Based on Eq. 5, we can form a new objective function for obtaining the best registration as follows:

$$h_2(\mathbf{T}) = \sum_{j=1}^m \left\| {}^u\mathbf{p}_j^C - \frac{\mathbf{n}_j^C(f_\beta)_j}{c_j} - \mathbf{T}({}^d\mathbf{p}_\beta^R)_j \right\|^2, \quad (6)$$

where $(f_\beta)_j$ and $({}^d\mathbf{p}_\beta^R)_j$ are the force and position measurements obtained by palpating the j^{th} undeformed points and m is the total number of undeformed points being probed. $\beta \in \{1, 2, \dots, l\}$ ($l \geq 2$) is the index of the measurement taken from the set of measurements at the j^{th} undeformed point.

The stiffness c_j is estimated from a pair of force-position measurements obtained by probing the undeformed point ${}^u\mathbf{p}_j^C$. The stiffness is estimated first from a pair of force-position measurements and then used to optimize $h_2(\mathbf{T})$. The objective function $h_2(\mathbf{T})$ is the difference in the squared norm of the distance between the estimated location of the deformed point and the sensed location of the deformed point.

It is to be noted from Eq. 6 that $h_2(\mathbf{T})$ only updates the registration and Eq. 4 updates the stiffness, unlike $h_1(\mathbf{x}_k)$ that is used to update both stiffness and registration (see Eq. 1). This results in an accurate stiffness estimate eliminating the issue of ambiguous registration estimate that we observe in [5].

If there are more than a pair of palpation points at the undeformed point ${}^u\mathbf{p}_j^C$, then we have the following:

$$\begin{aligned} c &= \frac{f_k}{d_k}, \quad k = 1, 2, \dots, l \quad (l \geq 2) \\ \Rightarrow c &= \frac{f_i - f_j}{d_i - d_j}, \quad i, j \in \{1, 2, \dots, l\} \text{ and } i \neq j. \end{aligned} \quad (7)$$

From Eq. 7, stiffness c linearly relates the depth ($d_i - d_j$) to the applied force ($f_i - f_j$). Thus we have $c = L(d_i - d_j, f_i - f_j)$, where L is the function that returns the slope of the best line fit through a regression on the data $\{(d_i - d_j, f_i - f_j)\}$.

Fig. 2 shows a flowchart that provides an overview of the various steps described so far.

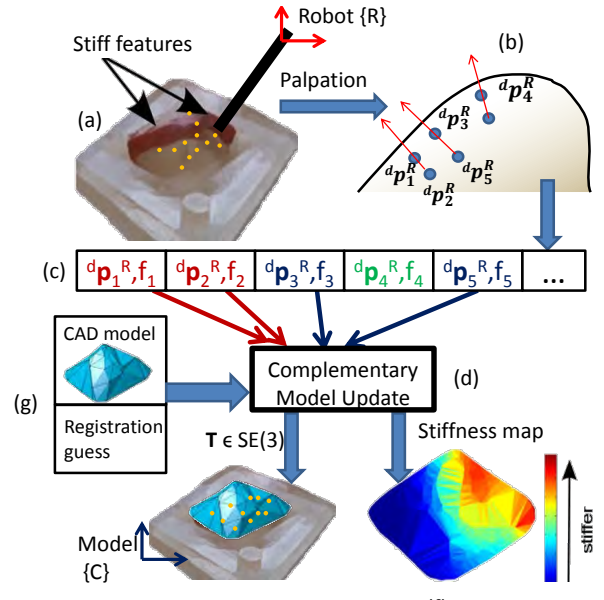


Fig. 2. Flowchart describing the inputs and outputs for complementary model update (a) Flexible environment with embedded stiff features is probed by a robot (b) Location of probed points are sensed (c) Compatible force-position measurements are collected (d) complementary model update estimates the registration and stiffness map (e) Robot frame and model frame are registered (f) Stiffness map is generated (g) Prior geometric model and the initial registration guess

The various steps involved in the CMU are listed below:

1) *Collection*: In the collection step, pairs of force-position measurements which satisfy the following conditions are grouped together in the same set:

- i The force magnitudes are different.
- ii The direction of normals fall within a threshold of each other.
- iii The position measurements fall within a threshold of each other.

The three conditions stated above imply that position measurements correspond to the same undeformed point being probed with different forces, and forming a compatible set. Given the measurements $({}^d\mathbf{p}_i^R, f_i)$, $i = 1, 2, \dots, n$ obtained so far, we collect compatible sets,

- $\{((^d\mathbf{p}_1^R)_j, (f_1)_j), ((^d\mathbf{p}_2^R)_j, (f_2)_j), \dots\}, j = 1, 2, \dots, m$, where m is the total number of distinct sets obtained.
- 2) *Stiffness estimation*: For each of the compatible sets that have at least one pair of force-position measurements, we estimate the local stiffness assuming a linear stiffness model as shown in Eq. 7.
 - 3) *Correspondence*: The points $(^d\mathbf{p}_\beta^R)_j$ are transformed using the best registration estimate available to obtain $(^d\mathbf{p}_\beta^C)_j$. We then find, $(^u\mathbf{p}_j^C, \mathbf{n}_j^C) = M((^d\mathbf{p}_\beta^C)_j, \phi)$, where M is the rule that finds the closest point $(^u\mathbf{p}_j^C) \in \phi$ to $(^d\mathbf{p}_\beta^C)_j$ and the corresponding normal \mathbf{n}_j^C . Other alternates for M include methods such as [20], [21].
 - 4) *Minimization*: The objective function described in Eq. 6 is minimized using a least squares solver [22], [23] or can be used in the update step of a Kalman filter [11] to estimate the registration.
 - 5) We loop between the Correspondence and Minimization step until convergence or upto a fixed number of iterations, upon obtaining T .

In the rest of this paper, we present results from an implementation of CMU that uses [23] for minimization; and we refer to such an implementation as SCAR-LSQ-CMU. We have also implemented a filtering approach using CMU, which will be referred to as SCAR-IEKF-CMU. But we do not present results of SCAR-IEKF-CMU due to space constraints.

The minimization step would only return a local minima when using a filter or least squares solver. One way to find global minima is to use a branch and bound technique as described in [12].

Algorithm 1: Complementary Model Update

Input:
 $^d\mathbf{p}_i^R \in \mathbf{R}^3, i = 1, 2, \dots, n$
 $f_i \in \mathbf{R}, i = 1, 2, \dots, n$
A priori CAD model: ϕ
Initial transformation: $T_0 \in SE(3)$
Output: Transformation T that aligns $^d\mathbf{p}_i^R$ with ϕ

- 1 **Collection**: Collect points satisfying compatibility criteria: $\{((^d\mathbf{p}_1^R)_j, (f_1)_j), ((^d\mathbf{p}_2^R)_j, (f_2)_j), \dots\}$
- 2 **Stiffness estimation**: Estimate the linear stiffness $c_j = L\left(\|(^d\mathbf{p}_\beta^R)_j - (^d\mathbf{p}_\gamma^R)_j\|, ((f_\beta)_j - (f_\gamma)_j)\right)$
Optimize Initialize: $T \leftarrow T_0$
- 3 **while not converged do**
- 4 **Correspondence**: $(^u\mathbf{p}_j^C, \mathbf{n}_j^C) = M((^d\mathbf{p}_\beta^C)_j, \phi)$
- 5 **Minimization**:

$$T = \underset{T}{\operatorname{argmin}} \sum_{j=1}^m \left\| ^u\mathbf{p}_j^C - \frac{\mathbf{n}_j^C(f_\beta)_j}{c_j} - T(^d\mathbf{p}_\beta^R)_j \right\|^2$$

V. SIMULATION STUDY

A. Comparison of SCAR-LSQ-CMU with SCAR-IEKF-old

In Fig. 3 we compare the results of SCAR-LSQ-CMU with SCAR-IEKF-old for a simulated case of a pyramid shaped

organ with an embedded stiff feature that was probed at 250 uniformly spaced points. The CAD model of the organ is represented in the form of a triangular mesh with 524 faces. We choose an initial guess for registration which is displaced along the Z direction by 4mm.

SCAR-LSQ-CMU accurately estimates the true registration after palpation of about 20 points. While SCAR-IEKF-old correctly estimates the translation components of registration (albeit not better than SCAR-LSQ-CMU), there is significant rotational error even after probing 250 points (see Table II).

TABLE II
REGISTRATION COMPARISON

	x (mm)	y (mm)	z (mm)	θ_x (deg)	θ_y (deg)	θ_z (deg)	RMS (mm)
Actual	0	0	0	0	0	0	–
SCAR-LSQ-CMU	0	0	0	0	0	0	0
SCAR-IEKF-old	0.32	0.12	2.46	-4.45	-1.03	1.22	5.66

The estimated stiffness map from SCAR-LSQ-CMU (see Fig. 3(b)) looks very similar to the ground truth stiffness map (see Fig. 3(a)), unlike the stiffness map estimated by SCAR-IEKF-old (see Fig. 3(c)). This example demonstrates how the CMU overcomes the ambiguity described in section IV and provides better estimates compared to SCAR-IEKF-old.

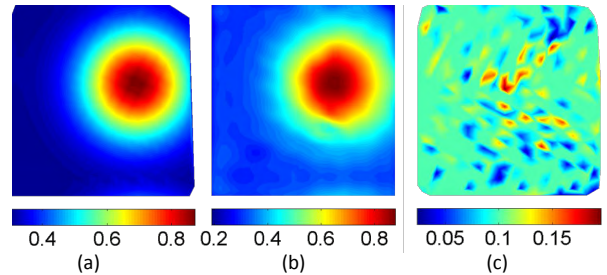


Fig. 3. Stiffness in N/mm (a) Ground truth (b) Estimated by SCAR-LSQ-CMU (c) Estimated by SCAR-IEKF-old

B. Evaluation with different levels of sensor noise

In order to test the robustness of the proposed algorithm to the presence of noise in the sensor measurements, we develop simulation data in which we artificially add noise to the measurements. We take the case of an organ whose shape is as shown in Fig. 6(a) with a synthetic ground truth stiffness map as shown in Fig. 4(a). The CAD model has 1311 triangle faces and is probed at 341 uniformly spaced points. At each palpated point, we record 10 measurements by probing along the normal up to a depth of 3mm in increments of 0.3mm. An artificial noise selected uniformly from $[0, 0.1]\text{mm}$ and $[0, 0.1]\text{N}$ is added to the sensed position and force respectively. Fig. 4(b) shows the stiffness map as estimated using SCAR-LSQ-CMU on this data. The stiffness map reveals the stiff features present in the ground truth. Following this we increase the noise in the sensed position, by

selecting uniformly from $[0, 0.3]$ mm. The stiffness estimation as shown in Fig. 4(c) demonstrates that SCAR-LSQ-CMU can reveal the stiff features even in the presence of high sensor noise.

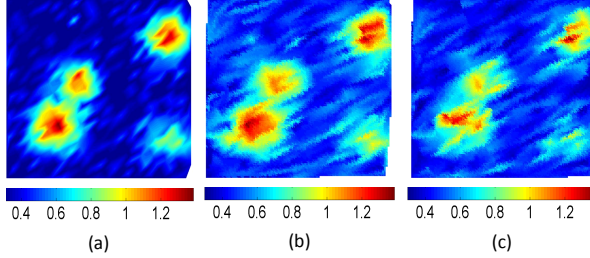


Fig. 4. Stiffness in N/mm(a) Ground truth (b) Estimated under low sensor noise (c) Estimated under high sensor noise

TABLE III
REGISTRATION RESULTS FOR DIFFERENT NOISE LEVELS

	x (mm)	y (mm)	z (mm)	θ_x (deg)	θ_y (deg)	θ_z (deg)	RMS (mm)
Low noise level							
Actual	7	-12	15	-11.46	5.72	8.59	—
SCAR-LSQ-CMU	6.99	-11.94	14.99	-11.46	5.73	8.56	0.02
ICP	6.40	-11.32	17.39	-11.28	5.35	8.36	2.33
DICP	8.69	-13.63	17.12	-11.22	5.89	8.53	3.00
High noise level							
SCAR-LSQ-CMU	6.99	-11.96	15.00	-11.48	5.72	8.56	0.02
ICP	7.15	-13.14	17.14	-11.44	5.80	9.06	2.35
DICP	8.59	-14.05	17.42	-11.30	5.94	8.87	3.24

Table III shows the comparison of the results as estimated by SCAR-LSQ-CMU with ICP [8], one of the most popular registration methods. Since ICP does not consider local deformations in its formulation, we create a modified formulation of the ICP to compensate for the local deformations (which we term deformation compensated ICP or DICP), so that we can provide a fair comparison to SCAR-LSQ-CMU. In DICP we estimate the local deformation from the stiffness data and then displace the probed points along the sensed normal by the deformation depth to estimate the undeformed points. Upon estimating the undeformed points, we use the original ICP to estimate the registration. In addition to finding the registration estimates, we also find the root mean square (RMS) error between the estimated positions and true positions, over all the probed points.

We assume the initial registration guess is $T_0 = I$, where I is an identity matrix. As expected, estimating local deformations results in SCAR-LSQ-CMU performing better than ICP and DICP in both the cases. DICP is affected by noise in sensed normal data resulting in a poor registration estimate, while SCAR-LSQ-CMU uses normal from the CAD model.

C. Exploration of robustness to initial registration error

For the simulated example presented in Section V-B with lower sensor noise, we evaluate the registration estimates for two different initial registration errors. The initial registration

error for Case 1 is lower than that for Case 2. From Table IV we observe that SCAR-LSQ-CMU estimates registration accurately even in the presence of high initial registration error.

TABLE IV
EXPLORATION OF ROBUSTNESS TO INITIAL CONDITIONS

	x (mm)	y (mm)	z (mm)	θ_x (deg)	θ_y (deg)	θ_z (deg)	RMS (mm)
Case1							
Initial	7.30	-12.10	15.61	-10.91	5.25	8.39	—
Actual	7	-12	15	-11.46	5.72	8.59	—
SCAR-LSQ-CMU	6.95	-11.94	14.99	-11.45	5.68	8.56	0.03
ICP	7.07	-12.25	16.26	-11.40	5.79	8.73	1.31
DICP	7.69	-11.86	16.21	-11.32	5.89	8.42	1.22
Case 2							
Initial	-13.31	-2.42	32.18	-30.76	-9.74	36.98	—
SCAR-LSQ-CMU	6.97	-11.91	15.01	-11.47	5.70	8.54	0.02
ICP	7.07	-12.25	16.26	-11.40	5.79	8.73	1.31
DICP	8.93	-11.93	16.51	-14.93	6.05	8.66	3.67

VI. EXPERIMENTAL VALIDATION

A. Experimental Setup

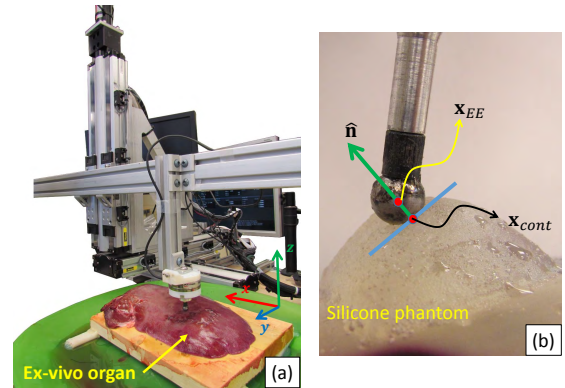


Fig. 5. (a) Cartesian robot setup for experiments (b) Contact location and surface norm estimation

To evaluate our CMU algorithm we have used a custom designed Cartesian robot with an open architecture controller (see Fig. 5(a)). The robot end-effector was equipped with an ATI Nano43 F/T sensor. A target machine using Matlab Simulink® Real-Time operating system was used for the low level control at a control frequency of 1 KHz. For the probing and environment exploration, a hybrid motion/force controller was implemented as in Khatib [24]. The motion control was accomplished using proportional derivative inverse dynamics controller with a 5th order polynomial trajectory generator. A proportional integral control law was used for force control. The force and motion reference commands were generated on a host machine which communicated with the low-level target machine using UDP.

B. Robot Automatic Probing Procedures

Given a target region for exploration, the host machine generates a uniformly distributed grid map (uniform spacing

in the $\hat{x}-\hat{y}$ plane of the robot) for probing locations. Given a particular reference probing location \mathbf{x}_p , the robot repeats the following steps to obtain the force-position measurements:

- 1) *Making high force contact*: The robot is first commanded to move to a desired position \mathbf{x}_p and then to move along the Z direction until a force magnitude 0.5N is reached.
- 2) *Estimating surface norm*: The surface normal $\hat{\mathbf{n}}$ is computed as the direction of the sensed force: $\hat{\mathbf{n}} = \mathbf{f}_s / \|\mathbf{f}_s\|$. The location of the contact point on the surface can be computed as: $\mathbf{x}_{\text{cont}} = \mathbf{x}_{\text{EE}} - \hat{\mathbf{n}}r$ (see Fig. 5(b)).
- 3) *Finding low force surface contact point*: The robot first retrieves swiftly away from the surface along the direction of the estimated normal and then moves slowly towards the surface along the normal till the sensed force reaches a threshold.
- 4) *Probing and recording*: The force and position measurements are recorded as the robot moves up to a preset depth into the organ under position control.

C. Results of probing silicone model with stiff features

We use a silicone phantom organ with embedded stiff features as shown in Fig. 6(a) to test the performance of SCAR-LSQ-CMU. The phantom is probed at 1010 uniformly spaced points. The stiffness map as estimated from SCAR-LSQ-CMU reveals all four stiff features (see Fig. 6(b)). Table V shows the registration estimates from SCAR-LSQ-CMU, ICP and DICP. From Fig. 6(c) we notice that SCAR-LSQ-CMU has a lower RMS error than ICP and DICP after about 25 iterations. We also observe that the estimate converges with as few as 100 points for SCAR-LSQ-CMU as opposed to ICP and DICP (see Fig. 6(d)). This suggests that even though we have 1010 probed points, for an accurate registration estimation we only need to probe about 100 points. A Bayesian optimization-based procedure to optimally choose these points to probe, has been recently developed by Ayvali et al [25].

TABLE V

REGISTRATION RESULTS FOR EXPERIMENTAL DATA

Silicone model	x (mm)	y (mm)	z (mm)	θ_x (deg)	θ_y (deg)	θ_z (deg)	RMS (mm)
Actual	5	-7	10	5.73	5.73	-8.59	-
SCAR-LSQ-CMU	4.96	-7.07	10.07	5.71	5.70	-8.50	0.11
ICP	4.96	-7.05	10.76	5.71	5.71	-8.51	0.80
DICP	6.67	-6.86	10.83	5.56	5.79	-8.79	1.87
<i>Ex vivo</i> organ							
Actual	7	8	-10	-5.73	-5.73	8.59	-
SCAR-LSQ-CMU	7.45	7.80	-9.81	-5.73	-5.48	8.69	0.28
ICP	5.56	7.39	-7.66	-0.43	-6.2	8.62	4.15
DICP	6.36	7.59	-9.66	-0.48	-5.84	8.52	3.49

D. Results of probing ex vivo organ

In order to validate the proposed work in a more realistic scenario, we palpate a porcine liver and use SCAR-LSQ-CMU for registration and stiffness estimation. A triangular plastic inclusion is artificially placed inside the

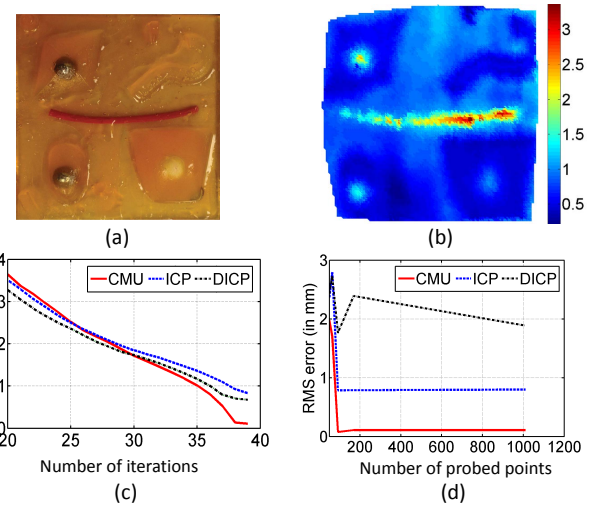


Fig. 6. (a) Top view of the silicone organ (b) Stiffness map as estimated by SCAR-LSQ-CMU (Stiffness in N/mm) (c) Comparison of RMS error vs number of iterations (d) Comparison of RMS error vs number of probed points

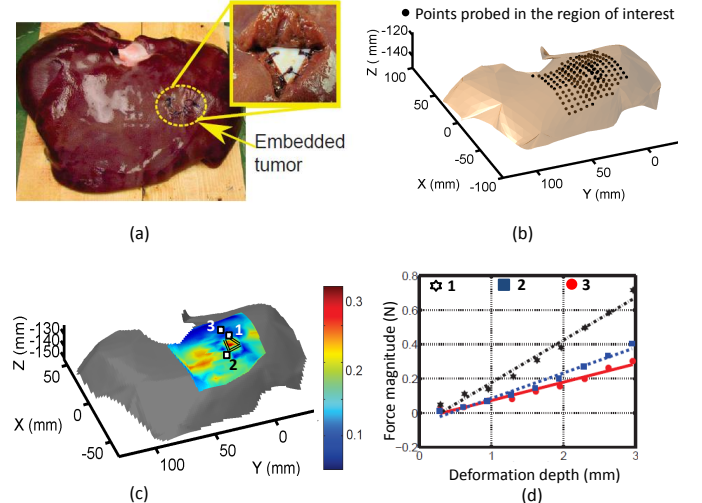


Fig. 7. (a) An *ex vivo* porcine liver with artificially embedded tumor (b) Position of probed points on the surface of the organ (c) Stiffness map as estimated by SCAR-LSQ-CMU (Stiffness in N/mm)(d) Variation of applied force with deformation depth at three arbitrarily points chosen in (c)

organ and sutured as shown in Fig. 7(a). We palpate a region of interest on the liver at 196 equally spaced points. In order to obtain the location of the inclusion, we manually probe the organ with an optical marker and track the position using a Polaris Vicra optical tracking system. We then place an optical marker on the tool tip to compare the position of the tool-tip in the tracker's frame as well as in the robot's frame to obtain the ground-truth registration.

We obtain a stiffness map as shown in Fig. 7(c), which clearly shows the stiff inclusion. Fig. 7(d) shows linear variation of force with depth at three arbitrarily chosen locations on the surface, validating our assumption of a linear stiffness model. Table V shows the registration estimates for an initial registration guess of $T_0 = \mathbf{I}$. The accuracy of

registration as required for clinical applications generally depends on the size of the smallest tumor that needs to be removed and the resection margin [26], [27]. In this example, the size of the tumor is 2cm and the registration accuracy obtained is 0.28mm. Hence we can safely say that the obtained registration accuracy is sufficient to discern the tumor.

VII. CONCLUSION

We have presented a new and robust formulation that uses mechanical palpation to simultaneously estimate the stiffness distribution and register preoperative models to visible anatomy. We believe the proposed model update is not a replacement but instead complementary to existing intraoperative registration methods. The performance of the new update method to several initial conditions, different geometries, stiffness profiles as well as sensitivity to sensor noise was evaluated and its robustness was demonstrated by a number of examples. We also introduce deformation compensated ICP (DICP) as an improvement over ICP, to provide a more fair comparison to SCAR-LSQ-CMU. We show that SCAR-LSQ-CMU performs better than SCAR-IEKF-old, DICP and ICP.

While we presented an implementation of this update model with a least squares optimizer in this paper it must be noted that the update model can be used with other optimizers as well as filtering approaches such as [5], [11], which forms part of future work. In this work, we use a simple experimental setup for evaluating our method, while avoiding additional sources of error such as robot deflection and positional errors typically seen in existing surgical systems. However, we plan to deploy our algorithm on research platforms that address key issues of surgical access constraints during MIS and offer force sensing capabilities.

REFERENCES

- [1] M. V. Wyawahare, P. M. Patil, H. K. Abhyankar, *et al.*, “Image registration techniques: an overview,” *International Journal of Signal Processing, Image Processing and Pattern Recognition*, vol. 2, no. 3, pp. 11–28, 2009.
- [2] M. Hayashibe, N. Suzuki, and Y. Nakamura, “Laser-scan endoscope system for intraoperative geometry acquisition and surgical robot safety management,” *Medical Image Analysis*, vol. 10, no. 4, pp. 509 – 519, 2006.
- [3] R. E. Goldman, A. Bajo, and N. Simaan, “Algorithms for autonomous exploration and estimation in compliant environments,” *Robotica*, vol. 31, pp. 71–87, 1 2013.
- [4] T. Yamamoto, M. Bernhardt, A. Peer, M. Buss, and A. M. Okamura, “Techniques for Environment Parameter Estimation During Telemanipulation,” in *Proceedings of the International Conference on Biomedical Robotics and Biomechatronics*, 2008, pp. 217–223.
- [5] S. Sanan, S. Tully, A. Bajo, N. Simaan, and H. Choset, “Simultaneous compliance and registration estimation for robotic surgery,” in *Proceedings of the Robotics: Science and Systems Conference*, 2014.
- [6] H. Liu, D. P. Noonan, B. J. Challacombe, P. Dasgupta, L. D. Seneviratne, and K. Althoefer, “Rolling mechanical imaging for tissue abnormality localization during minimally invasive surgery,” *IEEE Transactions on Biomedical Engineering*, vol. 57, no. 2, pp. 404–414, 2010.
- [7] M. Feuerstein, T. Mussack, S. Heining, and N. Navab, “Intraoperative laparoscope augmentation for port placement and resection planning in minimally invasive liver resection,” *IEEE Transactions on Medical Imaging*, vol. 27, no. 3, pp. 355–369, March 2008.
- [8] P. Besl and N. D. McKay, “A method for registration of 3-D shapes,” *IEEE Transactions on Pattern Analysis and Machine Intelligence*, vol. 14, no. 2, pp. 239–256, Feb 1992.
- [9] S. Rusinkiewicz and M. Levoy, “Efficient Variants of the ICP Algorithm,” in *Third International Conference on 3D Digital Imaging and Modeling (3DIM)*, June 2001.
- [10] P. Yan and K. W. Bowyer, “A Fast Algorithm for ICP-based 3D Shape Biometrics,” *Comput. Vis. Image Underst.*, vol. 107, no. 3, pp. 195–202, 2007.
- [11] M. H. Moghari and P. Abolmaesumi, “Point-based rigid-body registration using an unscented Kalman filter,” *IEEE Transactions on Medical Imaging*, vol. 26, no. 12, pp. 1708–1728, 2007.
- [12] J. Yang, H. Li, and Y. Jia, “Go-ICP: Solving 3D Registration Efficiently and Globally Optimally,” in *2013 IEEE International Conference on Computer Vision (ICCV)*, Dec 2013, pp. 1457–1464.
- [13] A. Myronenko and X. Song, “Point Set Registration: Coherent Point Drift,” *IEEE Transactions on Pattern Analysis and Machine Intelligence*, vol. 32, no. 12, pp. 2262–2275, Dec 2010.
- [14] A. Sotiras, C. Davatzikos, and N. Paragios, “Deformable Medical Image Registration: A Survey,” *Medical Imaging, IEEE Transactions on*, vol. 32, no. 7, pp. 1153–1190, July 2013.
- [15] R. Sagawa, K. Akasaka, Y. Yagi, and L. V. Gool, “Elastic convolved ICP for the registration of deformable objects,” in *IEEE 12th International Conference on Computer Vision Workshop*, 2009, pp. 1558–1565.
- [16] T. Lange, S. Eulensteiner, M. Hnerbein, and P.-M. Schlag, “Vessel-Based Non-Rigid Registration of MR/CT and 3D Ultrasound for Navigation in Liver Surgery,” *Computer Aided Surgery*, vol. 8, no. 5, pp. 228–240, 2003, pMID: 15529952.
- [17] A. Roche, X. Pennec, G. Malandain, and N. Ayache, “Rigid Registration of 3D Ultrasound with MR Images: a New Approach Combining Intensity and Gradient Information,” *IEEE Transactions on Medical Imaging*, vol. 20, pp. 1038–1049, 2001.
- [18] K. Lunn, K. Paulsen, D. Roberts, F. Kennedy, A. Hartov, and J. West, “Displacement estimation with co-registered ultrasound for image guided neurosurgery: a quantitative *in vivo* porcine study,” *IEEE Transactions on Medical Imaging*, vol. 22, no. 11, pp. 1358–1368, Nov 2003.
- [19] S. Ji, D. W. Roberts, A. Hartov, and K. D. Paulsen, “Intraoperative patient registration using volumetric true 3D ultrasound without fiducials,” *Medical Physics*, vol. 39, no. 12, pp. 7540–7552, 2012.
- [20] S. D. Billings, E. M. Boctor, and R. H. Taylor, “Iterative Most-Likely Point Registration (IMLP): A Robust Algorithm for Computing Optimal Shape Alignment,” *PLoS ONE*, vol. 10, 2015.
- [21] N. Ryan, C. Heneghan, and P. de Chazal, “Registration of digital retinal images using landmark correspondence by expectation maximization,” *Image and Vision Computing*, vol. 22, no. 11, pp. 883–898, 2004.
- [22] B. Horn, “Closed-form solution of absolute orientation using unit quaternions,” *Journal of the Optical Society of America A*, vol. 4, pp. 629–642, 1987.
- [23] K. Arun, T. Huang, and S. Bolstein, “Least-Squares Fitting of Two 3-D Point Sets,” *IEEE Transactions on Pattern Analysis and Machine Intelligence*, vol. 9, no. 5, pp. 698–700, 1987.
- [24] O. Khatib, “A unified approach for motion and force control of robot manipulators: The operational space formulation,” *IEEE Journal of Robotics and Automation*, vol. 3, no. 1, pp. 43–53, 1987.
- [25] E. Ayvali, R. A. Srivatsan, L. Wang, R. Roy, N. Simaan, and H. Choset, “Using Bayesian Optimization to Guide Probing of a Flexible Environment for Simultaneous Registration and Stiffness Mapping,” *The International Conference on Robotics and Automation*, 2016.
- [26] C. A. Linte, J. Moore, and T. M. Peters, “How accurate is accurate enough? a brief overview on accuracy considerations in image-guided cardiac interventions,” in *Annual International Conference of the Engineering in Medicine and Biology Society*. IEEE, 2010, pp. 2313–2316.
- [27] D. Vandeweyer, E. L. Neo, J. W. Chen, G. J. Maddern, T. G. Wilson, and R. T. Padbury, “Influence of resection margin on survival in hepatic resections for colorectal liver metastases,” *HPB*, vol. 11, no. 6, pp. 499–504, 2009.